The Astrophysical Journal, 578:897–913, 2002 October 20

THE INFRARED EMISSION OF CIRCUMSTELLAR ENVELOPES, DARK SILHOUETTES, AND PHOTOIONIZED DISKS IN H II REGIONS

M. Robberto,[1] S. V. W. Beckwith, and N. Panagia[1]
Space Telescope Science Institute, 3700 San Martin Drive, Baltimore, MD 21218;
robberto@stsci.edu, svwb@stsci.edu, panagia@stsci.edu
Received 2001 November 30; accepted 2002 July 1

ABSTRACT

We have modeled the infrared (IR) spectral energy distribution (SED) of circumstellar disks embedded in a H II region and photoevaporated by the external ultraviolet radiation. The model applies to the photoevaporated disks (proplyds) in the Orion Nebula, most of them illuminated by the O6.5 star θ^1 Ori C. First we calculate the IR emission of a pre–main-sequence star surrounded by a dusty globule that is immersed within an H II region. The globule is assumed to be spherical, homogeneous, optically thin at IR wavelengths, and photoevaporated according to the Dyson model. Second, we consider the IR emission of a disk directly exposed to the nebular environment. The reprocessing disk is passive and treated according to the Chiang & Goldreich model. We improve over the Chiang & Goldreich treatment by tracing the propagation of the various radiative fluxes (from the star exciting the H II region, nebular, and grazing from the disk central star) through the disk superheated atmosphere. Since the opposite disk sides receive different amounts of radiation, the flaring angle and the surface temperature distributions are different, resulting in well-distinguished SEDs for the two disk faces. Finally, we combine the globule and disk models to estimate the IR emission of proplyds. The energy input from the central star and the nebular environment increase the disk flaring angle, and therefore also the amount of stellar radiation intercepted by the disk. The relative intensity of the disk versus envelope emission varies with the tilt angle relative to the directions of θ^1 Ori C and the Earth. We explore the dependence of the SEDs upon the tilt angle with respect to the Earth, the distance from θ^1 Ori C, the size on the envelope, the inner disk radius, and the temperature of the central star. The resulting SEDs are characterized by a broad peak of emission at 30–60 μm and are in general significantly different from those of isolated disks in low-mass star-forming regions like Taurus-Auriga. Our model indicates that in the presence of an external radiation field, relatively evolved Class 2 objects may display a SED peaking at mid-IR and far-IR wavelengths. Also, the model can account for the strong mid-IR excess we have recently detected at 10 μm from embedded disks in the Orion Nebula.

Subject headings: accretion, accretion disks — infrared: stars — ISM: individual (Orion Nebula) — stars: pre–main-sequence

1. INTRODUCTION

Circumstellar disks are thought to be the birth sites of planetary systems, and it is primarily for this reason that their properties have been studied extensively since the early 1980 s (Shu, Adams, & Lizano 1987; Beckwith & Sargent 1996; Hartmann 1998). The discovery of several tens of extrasolar planetary systems (e.g., Marcy, Cochran, & Mayor 2000) added weight to the argument that disks create planets, although there is some debate about how often planetary systems really occur around stars. Nevertheless, an understanding of the evolutionary properties of disks around young stars is thought to be an essential part of the understanding of our own origins.

Disks can also affect the early evolution of stars themselves. Several authors have suggested that stellar rotation is locked to the orbital rates of the inner disks at early times, allowing the disk to regulate the stellar angular momentum (Edwards et al. 1993; Choi & Herbst 1996), although this idea is still controversial (Stassun et al. 1999; Rebull 2001). Typical disk masses and accretion rates appear to be too small to greatly change the mass of the stars through accretion (Palla & Stahler 1999). A number of observable characteristics of young star/disk systems play an important role in determining the stellar properties, and therefore understanding even subtle changes is important to ensure that the stellar properties are correctly interpreted.

Most of the stars in the Galaxy are thought to be born in dense OB clusters such as the Orion Nebula (Bally et al. 1998a; McCaughrean & Stauffer 1994). However, our understanding of circumstellar disks comes mainly from studies of nearby dark clouds such as the Taurus/Auriga complex, and it is not clear that the extant knowledge of circumstellar disks applies to the majority of young star/disk systems in the Galaxy. The study of the disks in Orion presents several problems that have slowed progress: they are seen against the Orion H II region, a bright, highly nonuniform source of radiation at wavelengths from the ultraviolet through millimeter; they appear to be fainter on average at millimeter wavelengths (Bally et al. 1998b); and the Orion nebula is 3 times farther from the Earth than the well-studied dark clouds. Many of the disks are embedded within the H II region, meaning that they are surrounded by ionized halos of gas and dust that complicate the observation of disk properties alone.

To address these difficulties, we present in this paper a series of models of the emission from disks embedded

[1] On assignment from the Space Telescope Operations Division of the European Space Agency (ESA).

within the Orion H II region, under the influence of other radiation sources in addition to the stars at their center. Section 2 is a discussion of various sources of radiation in the H II region to prepare for the calculations of emission from discrete sources. In the following sections, we show how the different radiation affects the IR emission arising from three type of sources: a spherically symmetric, dusty globule surrounding a star (§ 3), a star/disk system directly exposed to the ionized environment (§ 4), and finally a star/disk system surrounded by a dusty globule (§ 5). Section 6 contains a discussion of our findings with an exploration of the critical parameters, comparison with observations, and remarks on the limit of our treatment.

2. GENERAL PARAMETERS OF THE H II REGION

We assume the H II region is spherical, isothermal, and has uniform density. For simplicity, we consider the brightest star at its center as the only source of ionizing photons, neglecting the radiation emitted by other stars within or around the nebula. This approximation is appropriate for the Trapezium Custer, where θ^1 Ori C supplies at least 80% of the Lyman continuum luminosity: $L_{\rm Lyc} \approx 8 \times 10^4\ L_\odot$ versus a total luminosity of $\sim 10^5\ L_\odot$ for the entire cluster (Bally et al. 1998a). We assume the H II region is radiation-bounded with Strömgren radius, $R_{\rm H\,II}$, i.e., all the Lyman continuum radiation is absorbed within the nebula. We use for the H II region the typical parameters of the Orion Nebula, with a Strömgren radius $R_{\rm H\,II} = 1 \times 10^{18}$ cm and a distance $D = 450$ pc.

To estimate the relative importance of the various dust-heating mechanisms, it is appropriate to distinguish between the stellar, F_s, and the nebular, F_n, radiative fluxes (Panagia 1974; Natta & Panagia 1976). The stellar flux is comprised of ionizing, $F_s^{\rm EUV}$, and nonionizing, $F_s^{\rm FUV}$, radiation. The former maintains the ionization balance and is mostly absorbed in the vicinity of the Strömgren boundary. Once absorbed, it is transformed into nebular radiation, F_n, that fills the H II region uniformly. F_n can be divided into the resonantly scattered Lyα radiation, $F_n^{\rm Ly\alpha}$, and the rest, e.g., Balmer continuum and lines, forbidden lines from various atomic species, continuum emission, etc., for short all referred to hereafter as nebular radiation and indicated by $F_n^{\rm other}$.

If ρ denotes the fraction of total luminosity, L_s, emitted by the central star in the Lyman continuum (EUV; $h\nu > h\nu_{\rm Lyc} = 13.6$ eV), the ionizing flux at a distance, d, is

$$F_s^{\rm EUV}(d) = \rho \frac{L_s}{4\pi d^2} e^{-\tau_{\rm EUV}(d)} , \quad (1)$$

where $\tau_{\rm EUV}(d)$ is the radial optical depth at the effective wavelength of the ionizing radiation, $\lambda_{\rm EUV}$ ($\sim$570 Å for θ^1 Ori C). The nonionizing stellar radiation (FUV; $6\ {\rm eV} < h\nu < 13.6\ {\rm eV}$) is

$$F_s^{\rm FUV}(d) = (1-\rho) \frac{L_s}{4\pi d^2} e^{-\tau_{\rm FUV}(d)} , \quad (2)$$

with an effective wavelength $\lambda_{\rm FUV} \simeq 1200$ Å (Panagia 1974).

With the exception of the dusty globules and disks, discussed later in this paper, we assume that the amount of dust mixed with the ionized gas is negligible, so that both the EUV and FUV fluxes cross the H II region almost unaffected by dust.

Recombination theory predicts that as long as the electron density is $\ll 10^4\ {\rm cm}^{-3}$, a fraction $\simeq \frac{2}{3}$ of the Ly continuum photons are eventually transformed into Lyα photons at $\lambda_{\rm Ly\alpha} = 1216$ Å through the $2p$–$1s$ transition, the remaining decaying to $1s$ via two-photon emission from the $2s$ level (e.g., Osterbrock 1989). The generation rate of Lyα photons is therefore

$$N^{\rm Ly\alpha} \cong \frac{2}{3} \frac{\rho L_s}{h\nu_{\rm Lyc}} , \quad (3)$$

and the corresponding luminosity is

$$L_n^{\rm Ly\alpha} \cong \frac{2}{3} \rho L_s \left(\frac{\lambda_{\rm Lyc}}{\lambda_{\rm Ly\alpha}} \right) \simeq \frac{1}{3} \rho L_s , \quad (4)$$

where $\lambda_{\rm Lyc} = c/\nu_{\rm Lyc} = 912$ Å. For the ionizing star we adopt the parameters of an O6.5 V star: $L_s = 6 \times 10^{38}$ ergs s^{-1} and $\rho = 0.4$ (Panagia 1973).

For the remaining nebular radiation,

$$L_n^{\rm other} = \rho L_s - L_n^{\rm Ly\alpha} \simeq \tfrac{2}{3} \rho L_s . \quad (5)$$

The energy density of the nebular radiation is obtained by multiplying the luminosity by the crossing time, $R_{\rm H\,II}/c$, and dividing by the nebular volume, $V_{\rm neb} = (4/3)\pi R_{\rm H\,II}^3$. In the case of the Ly$\alpha$ radiation, the photons are resonantly scattered many times within the nebula before being absorbed. Numerical models (Panagia 1978; Hummer & Kunasz 1980) indicate that whereas Lyα photons undergo approximately 10^5 scatterings before reaching the boundary of an H II region, the space crossed between most of the scatterings is very short, so that a Lyα photon reaches the boundary after having traveled on average a path length about $q \sim 10$–20 times the radius of the H II region. Therefore, the absorption of Lyα photons by dust is about q times more efficient than it is for nonresonant radiation with similar frequency. From the point of view of the dust heating by Lyα radiation, the factor, q, can be treated either as an apparent increase of the Lyα energy density seen by the dust,

$$U_n^{\rm Ly\alpha} = \frac{q \rho L_s}{4\pi c R_{\rm H\,II}^2} , \quad (6)$$

or as an increase of the dust absorption efficiency $Q_{\rm abs}$ at the Lyα wavelength,

$$Q_{\rm abs}({\rm Ly}\alpha) = q Q_{\rm abs}({\rm UV}). \quad (7)$$

This second approach is more correct, since the apparent increase of the energy density holds only as long as Lyα photons are present, i.e., inside a dust-depleted H II region and at the outer edges of any embedded globule, disk, etc. In these objects, Lyα photons will cause an increase of the surface temperature, but at an optical depth to UV radiation $\tau \simeq 1$ they will be entirely absorbed. Equation (7) has been adopted in the rest of this paper.

Concerning the nebular radiation, one has

$$U_n^{\rm other} = \frac{2 \rho L_s}{4\pi c R_{\rm H\,II}^2} . \quad (8)$$

3. CIRCUMSTELLAR GLOBULES

3.1. *Neutral Flow*

The ionized globules in the central part of the Orion Nebula are typically shaped like teardrops with the tail pointing away from θ^1 Ori C. For simplicity, we treat them as spheres of neutral gas surrounded by a shell that is photoionized on the hemisphere facing the ionizing star. Johnstone, Hollenbach, & Bally (1998) and Störzer & Hollenbach (1999) have modeled the structure of the globules in terms of photoevaporated winds. They showed that two different outflow regimes may develop: EUV- and FUV-dominated flows. The former are produced when the ionizing radiation reaches the disk surface, typically in the vicinity ($d \lesssim 10^{17}$ cm) of the ionizing star, and/or in the very early phases of disk exposure to the EUV radiation. FUV-dominated flows are more common and occur when the EUV flux is absorbed at large distances from the disk surface. In this case, the disk photoevaporation is driven by the FUV radiation. The photodissociation region (PDR) that develops between the disk surface and the ionization front may extend hundreds of astronomical units, or a few disk radii ($\sim$100 AU), from the disk. Typical solutions of the flow equations indicate that in EUV-dominated flows the density remains approximately constant, whereas in FUV-dominated flows the expanding neutral flow has nearly constant velocity until it reaches an isothermal shock, which separates the inner region with density $\propto r^{-2}$ from the isobaric upstream region where the density is approximately constant.

Störzer & Hollenbach (1999) have shown that in most FUV-dominated cases the shock front occurs much closer to the central star than to the ionization front. The region with constant density therefore fills most of the globule's volume. The dense inner flow may still dominate the radial column density, but it is generated in the outer disk regions, where the thermal supersonic neutral wind at 2–6 km s^{-1} exceeds the escape velocity from the rotating disk. The neutral outflow will be initially cylindrical by symmetry, while a spherical flow develops only at distances of the order of the disk size. The star should therefore remain in a cavity relatively free of dust, possibly dominated by the presence of collimated jets (Bally, O'Dell, & McCaughrean, 2000). In conclusion, both EUV- and FUV-dominated flow models predict the presence of broad regions around the central star with uniform density. We shall therefore consider only FUV-dominated flows with constant density. Our neutral region spans from the ionization radius R_i down the an inner radius R_0, encircling a dust-free cavity set by the dust evaporation temperature, $T_e = 1500$ K. We shall refer to this structure as a "neutral globule."

The density within the proplyds is regulated by the dust opacity to the FUV flux (Bally et al. 1998a). If the density—and therefore, opacity—increases, the number of FUV photons reaching the disk diminishes. The smaller number of FUV photons causes the evaporation rate to drop with a consequent decrease of the density (opacity) in the globule. More FUV photons will then be able to reach the disk, keeping the system in equilibrium through negative feedback. Both Johnstone et al. (1998) and Störzer & Hollenbach (1999) estimated the column density of the neutral medium, $N(\mathrm{H}) \simeq 10^{21}$ cm^{-2}, corresponding to $A_V \simeq 0.5$ assuming average interstellar medium opacity. This column density translates into a radial optical depth $\tau_{R_i} \simeq 1$–2 in the UV (both EUV and FUV), the exact value depending on the dust properties. In the next section we shall see how τ_{R_i} is directly related to the ionizing flux and to the radius of the globule.

3.2. *Photoionized Wind*

Behind the ionization front, the gas flow is approximately spherically symmetric. At large distances from the globule, the interaction with the wind from the ionizing star will create the characteristic stationary arcs of [O III]+Hα emission seen around several sources in the inner core of the Orion Nebula (Bally et al. 1998a, 2000). Dust is trapped within the photoevaporating flow, as demonstrated by the arcs closer to θ^1 Ori C, which are prominent at 10 μm. In fact, the Ney-Allen Nebula is mostly due to the optically thin emission of dust in these arcs (Hayward, Houck, & Miles 1994).

Dyson (1968) first studied the evaporation of dense neutral globules in H II regions as a mechanism to provide high turbulence to the ionized medium. In Dyson's model, the globules are self gravitating spherical condensations of neutral hydrogen. Under the influence of the ionizing radiation, the ionized material at the globule surface streams out at supersonic velocities, injecting momentum and energy into the H II region. In this model, the spherically symmetric, steady flow has a solution given by

$$\frac{r}{R_i} = \sqrt{\frac{c_{\mathrm{II}}}{v(r)}} \exp\left[\frac{v(r)^2 - c_{\mathrm{II}}^2}{4c_{\mathrm{II}}^2}\right] \tag{9}$$

and

$$\frac{n(r)}{n_i} = \exp\left[\frac{c_{\mathrm{II}}^2 - v(r)^2}{2c_{\mathrm{II}}^2}\right], \tag{10}$$

where r is the distance from the center of the globule, $n(r)$ and $v(r)$ are the flow density and velocity, and n_i is the atomic density at R_i. We assume $c_{\mathrm{II}} = 10^6$ cm s^{-1} for the sound speed in the ionized gas. The Dyson solution neglects the role of gravity. In our case, gravity is negligible at distances from a central star $r \gtrsim 100$ AU, since the escape velocity, $v_e = (GM_*/r)^{1/2} \simeq 1$ km s^{-1}, for a central star of mass $M_* = 1\ M_\odot$ is significantly lower than c_{II} (see also Henney et al. 1996; Johnstone et al. 1998). In any case, the emitted IR spectrum is almost insensitive to the details of the density and velocity profiles.

In the expanding ionized flow, the neutral hydrogen and the grains compete for the absorption of the ionizing photons. The effects of dust in the photoevaporation flow has been studied by Pastor, Cantó, & Rodriguez (1991), and we refer the reader to their paper for the details. The optical depth within the globule is given by their equation (12),

$$F = n_i c_{\mathrm{II}} e^{\tau_d^\infty} + \alpha_B n_i^2 R_i b(\tau_d^0), \tag{11}$$

valid in the plane-parallel approximation, relating the flux of ultraviolet photons entering the globule, F, to the opacity from the ionization front to infinity, τ_d^∞, to $\tau_d^0 = \sigma_d n_i R_i$. Here α_B is the recombination coefficient to the excited levels of the hydrogen and $\sigma_d = 2 \times 10^{-21}$ cm^{-2} is the grain cross section per hydrogen nucleus to the EUV radiation. The function, $b(\tau_d^0)$, has been tabulated by Pastor et al. (1991) for the Dyson's density profile. When $\tau_d^0 \leq 10$, one can

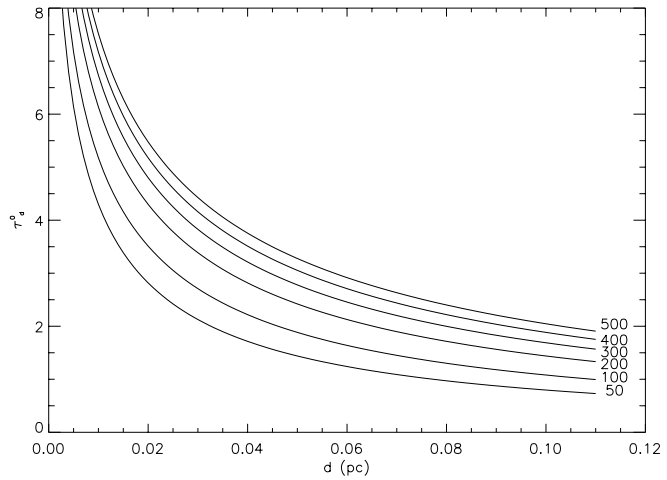

FIG. 1.—Optical depth $\tau_d^0 = \sigma_d n_i R_i$ as a function of the distance d from θ^1 Ori C. Six different globules are considered, with ionization front at $R = 50$, 100, 200, 300, 400, and 500 AU.

approximate

$$b(\tau_d^0) = 0.12e^{0.37\tau_d^0} . \quad (12)$$

In this case (Pastor et al 1991),

$$\tau_d^\infty = 0.45\tau_d^0 . \quad (13)$$

Figure 1 shows how the optical depth, τ_d^0, depends on the ionizing flux (i.e., distance from the ionizing star) and on the radius of the ionization front (i.e., globule's size) through equations (11)–(13). In general, τ_d^0 increases with the globule size and decreases with the ionizing flux. At distances from the ionizing star larger than 0.06–0.08 pc, it is $\tau_d^0 \simeq 1$–2. This corresponds to the range of values for τ_{R_i} mentioned above. In fact, under the assumption that the neutral, inner part of the globule has constant density, and as long as $R_0 \ll R_i$, τ_d^0 coincides with the radial optical depth τ_{R_i}. In this case, equation (11) links τ_{R_i} to the ionizing flux and to the globule radius. Both parameters can be easily obtained, or constrained, by the observations.

3.3. *Radiation Field inside the Globule*

Assuming the number density of globules present within the H II region to be low enough that each one of them is directly exposed to the radiation coming from the central star, the primary sources of energy within a globule of radius R will be the following:

1. The radiation (both ionizing and nonionizing) from the star exciting the H II region:

$$L_g^s(d) = L_s \frac{R^2}{4d^2} . \quad (14)$$

2. The diffuse radiation, including both Lyα and other nebular radiation:

$$L_g^{\rm nebular} = \frac{3}{4}\rho L_s \left(\frac{R}{R_{\rm H\,II}}\right)^2 . \quad (15)$$

3. The radiation L_* from the star at the center of the globule.

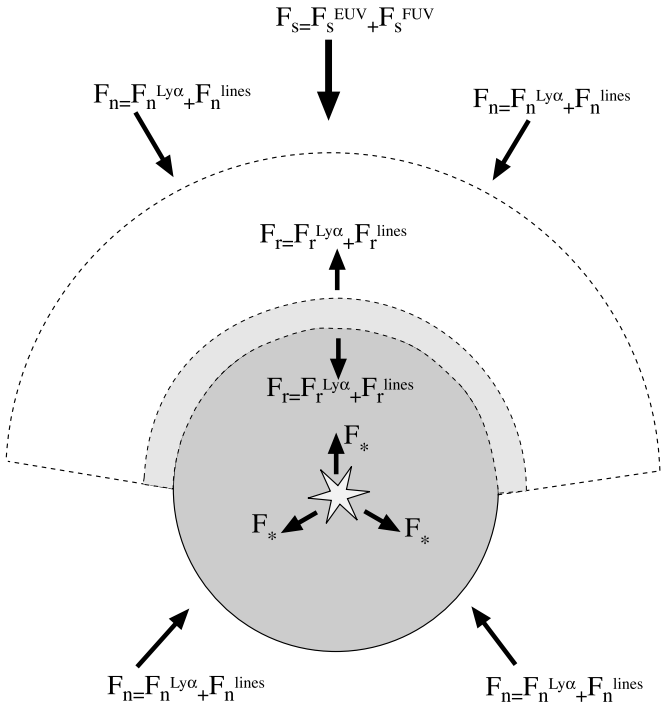

FIG. 2.—Sketch of our assumed globule geometry with the radiative fluxes relevant for the dust heating.

Within the globule, the energy density results from a combination of these three terms, plus the thin shell discussed in the previous section, each one attenuated by the dust and gas absorption. Note that now the first term dominates over the second at distances $d \le R_{\rm H\,II}/\sqrt{3\rho} \simeq 0.9R_{\rm H\,II}$. We neglect the IR radiation produced by the globule itself as a significant source of dust heating. Figure 2 provides a sketch of the contributions we are going to consider, beginning with the ionized wind. We shall assume hereafter $R \simeq R_i$.

3.3.1. *Ionized Wind*

Figure 3 illustrates how, according to the model described in the previous section, the UV flux is absorbed by the gaseous and dusty components within the ionized wind. We have assumed $d = 0.1$ pc, corresponding to $\simeq 45''$ at the distance of the Orion Nebula and $R_i = 100$ AU. With this choice of parameters, the FUV radiation is only $\approx$35% absorbed before reaching the ionization front. The FUV radiation also traces the fraction of EUV radiation absorbed by the dust.[2] The dust optical depth, depending linearly on the density, dominates the absorption of EUV photons for distances larger than $r \approx 1.3R_i$. When the gas optical depth (proportional to n^2) becomes dominant, the ionizing flux has already been reduced by approximately one half. The fraction of EUV radiation intercepted by the gas is therefore predominantly absorbed in a relatively thin layer outside the ionization front. The layer acts as a secondary source of recombination radiation, trapped between the neutral PDR region inside and the ionized wind outside. Each side receives 50% of the recombination radiation,

[2] In this paper we assume $Q_\nu = 1$ for the dust absorption efficiency in the EUV, FUV, Lyα, and nebular radiation. The corresponding optical depths are therefore equal.

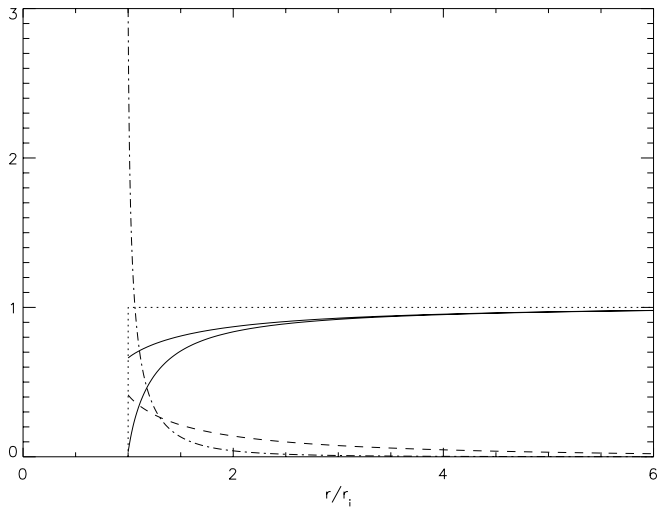

FIG. 3.—Propagation of the flux from θ^1 Ori C within the ionized wind. The two solid lines represent the FUV flux (*upper line*) and the EUV flux (*lower line*). The dashed line represents the dust optical depth, whereas the dot-dashed line represents the gas optical depth. The dotted line represents the ionization fraction.

again with Lyα carrying $\simeq\frac{1}{3}$ of the energy and FUV and optical lines carrying the rest. A crude estimate indicates that the flux emitted in each direction is approximately $\frac{1}{2}\times\frac{1}{2}\times\frac{1}{2}=\frac{1}{8}$ of the flux directly coming from the ionizing star, the three factors accounting for the fraction of the energy emitted in the EUV, the fraction of EUV radiation absorbed by the shell, and the fraction of photons emitted up/downstream. This amount is not negligible and has been included in the model.

We treat the radiative flux within the ionized wind in a one-dimensional approximation. The flux, F_s, coming from the ionizing star has a cylindrical symmetry along the globule axis, defined by the line joining the globule center to the ionizing star and equations (1) and (2) can be used with the optical depth, τ_d^∞, introduced in § 3.2. The nebular radiation flux, F_n, as well as the radiation produced at the ionization front, $F_{\rm if}$, are regarded as uniform, extended sources at the outer and inner edge of the ionized region, respectively. Treating the dusty region as a plane parallel slab illuminated by two uniform radiation fields, we use the attenuation averaged over 2π steradian:

$$\langle e^{-\tau}\rangle_{2\pi}=\int_0^1 e^{-\tau/x}\,dx\ . \tag{16}$$

In general, all nebular Lyα photons entering the ionized wind will be rapidly absorbed by the dust, whereas a fraction, $\langle e^{-\tau_d^\infty}\rangle_{2\pi}$, of the nebular radiation will cross the region.

To these terms, we add, together with the flux from the central star, F_*, the fraction of nebular recombination lines, Lyα excluded, coming from the back side after crossing the neutral globule.

3.3.2. *Neutral Globule*

Within the neutral region, we use a two-dimensional treatment. No EUV radiation is present, and the fraction of FUV radiation crossing the ionization front is further attenuated by an optical depth,

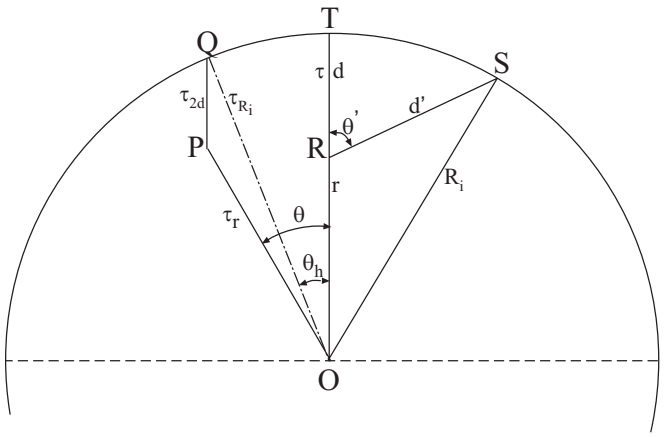

FIG. 4.—Globule geometry. The left side shows our naming conventions for the optical depths, the right side for the distances. There is a simple relation between optical depth and distance (eq. [18]), and corresponding quantities share the same index. Note, however, that τ corresponds to the distance $R_i - r$.

$$\tau_{2d}(r,\theta)=\tau_{R_i}\left[1+\left(\frac{r}{R_i}\right)^2-2\left(\frac{r}{R_i}\right)\cos(\theta-\theta_h)\right]^{1/2}, \tag{17}$$

between the point $Q(\theta_h)$ at the globule surface and the point $P(r,\theta)$, along the line parallel to the globule axis. It is $\theta_h=\arcsin[r\sin\theta/R_i]$ (Fig. 4). Note that since the globule is homogeneous, distances and optical depths are related by the simple relation

$$\tau_r=\tau_{R_i}\frac{r}{R_i}\ . \tag{18}$$

On the hemisphere facing the ionizing star, the ionized shell converts UV photons into recombination line photons. Like the ionized wind, the neutral globule is optically thick to Lyα photons and translucent to recombination lines at the range of optical depths we are dealing with. To illustrate their propagation, we consider first the energy input, E, from an isotropic radiation field with specific intensity, I_ν, on the surface of radius, R_i:

$$E_\nu=(4\pi R_i^2)\pi I_\nu\ . \tag{19}$$

Within the globule, the radiation field is attenuated by a factor

$$\langle e^{-\tau'(r)}\rangle_{\rm sphere}=\tfrac{1}{2}\int_0^\pi e^{-\tau'(r,\theta')}\sin\theta'\,d\theta'\ , \tag{20}$$

where $\tau'(r,\theta')$ is the optical depth between the point R, assumed for simplicity on the globule axis ($\theta=0$) and a point $S(\theta')$ on the surface (see Fig. 4). Figure 5 shows that when the globule is optically thick, the energy density at the center goes to zero, whereas at the surface it approximates 50% of its value in the open space, as the flux comes only from the outer side. Continuity across the globule edge is preserved, as the outer energy density is also reduced in the globule shadow with respect to the value in open space. The attenuation in the vicinity of the surface can then be estimated integrating equation (20) between 0 and $\pi/2$ in the limit $\tau_{R_i}\gg\tau$, τ being the radial optical depth from the surface. In this case, equation (20) reduces to equation (16).

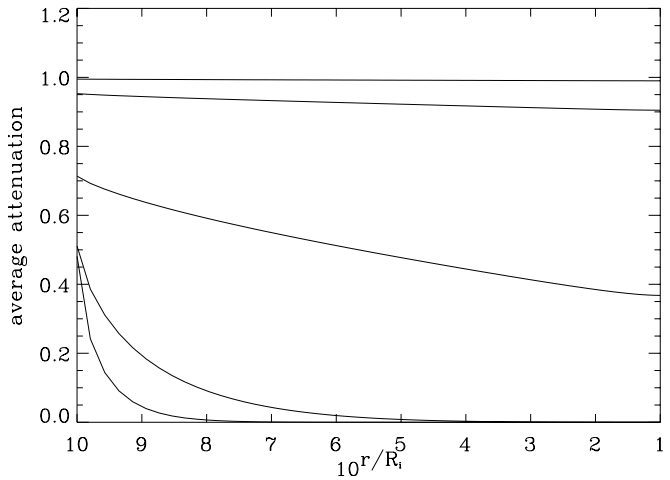

FIG. 5.—Attenuation of an isotropic radiation field within a homogeneous spherical globule with radial optical depth τ_R. *Top to the bottom:* $\tau_{R_i} = 0.01, 0.1, 1, 10$, and 30.

Since the two hemispheres are illuminated by different sources of radiation, isotropy is broken and equation (20) must be replaced by an equation weighting the two contributions separately. The flux at a point P will now depend also on the angle θ (see Fig. 4). It is convenient to write equation (19) as

$$E_\nu = \pi a^2 (4\pi I_\nu) \, , \tag{21}$$

and split the isotropic flux intercepted by the sphere cross section in two terms:

$$4\pi I_\nu = \Omega_1 A_1 I_\nu^1 + \Omega_2 A_2 I_\nu^2 \, . \tag{22}$$

Here Ω_i are the solid angles subtended by the areas radiating with intensity, I_i, and A_i are the corresponding mean attenuations. It is

$$A_1(r,\theta) = \langle e^{-\tau'(r,\theta)} \rangle_{up} = \frac{1}{4\pi} \times \left[\int_0^{2\pi} \int_0^{\theta'_{2\pi}(r,\theta,\phi')} e^{-\tau'(r,\theta,\theta',\phi')} \sin(\theta') d\theta' d\phi' \right] \tag{23}$$

and

$$A_2(r,\theta) = \langle e^{-\tau'(r,\theta)} \rangle_{\rm down} = \frac{1}{4\pi} \times \left[\int_0^{2\pi} \int_{\theta'_{2\pi}(r,\theta,\phi')}^{2\pi} e^{-\tau'(r,\theta,\theta',\phi')} \sin(\theta') d\theta' d\phi' \right] . \tag{24}$$

The optical depth, $\tau'(r,\theta,\theta',\phi')$, between the point, $P(r,\theta)$, inside the globule and a point, $S(\theta',\phi')$, on the surface of the sphere is related through equation (18) to r', solution of the equation

$$r'^2 + 2r(\cos\theta\cos\theta' + \sin\theta\sin\theta'\cos\phi')r' + r^2 - R^2 = 0 \, , \tag{25}$$

whereas the angle, $\theta'_{2\pi}(r,\theta,\phi')$, at P between the direction of the ionizing star, and the globule's equator is given by the equation

$$r^2\cos^2\theta\tan^2\theta'_{2\pi} - 2r^2\sin\theta\cos\theta\cos\phi'\tan\theta'_{2\pi} + r^2\sin^2\theta - R^2 = 0 \, . \tag{26}$$

3.3.3. *Flux from the Central Star*

The flux from the central star depends on r^{-2} and on the radial extinction. Since the central stars of the proplyds in the Orion Nebula typically have late spectral types, we account for the corresponding reduction of the dust optical depth through the ratio of absorption efficiencies $Q(\lambda_{T_*})/Q_{\rm UV} \cong Q(\lambda_{T_*})$, where λ_{T_*} is the effective wavelength of the photospheric radiation. At distances larger than R_0, the stellar flux is

$$F_*(r) = \frac{L_*}{4\pi r^2} e^{-\tau_r(r)Q(\lambda_{T_*})} \, , \tag{27}$$

where τ_r is the radial optical depth from the central star. Figure 6 shows the flux densities along the symmetry axis for a globule again with $R_i = 100$ AU and $d = 0.1$ pc. For the star, we assumed $T_* = 4000$ K and $R_* = 2.5\ R_\odot$. We shall refer hereafter to these values as the standard case. Within the ionized wind, the dust heating is dominated by the FUV flux. Inside the globule, the dominant source of heating is the radiation from the central star, in the inner parts, and the Lyα radiation closer to the ionization front.

3.4. *Infrared Emission*

The dust temperature, $T_d(r,\theta)$, is determined by the local energy balance of dust grains. Within the neutral part of the globule, it is given by the equation

$$\sigma_g \{ Q_{\rm UV}[F_{\rm FUV}(r,\theta) + F_{\rm Ly\alpha}(r,\theta)] + F_{\rm REC}(r,\theta) + Q(\lambda_{T_*})F_*(r)\} = 4\sigma_g \int_0^\infty Q(\nu)\pi B[\nu, T_d(r,\theta)] d\nu \, , \tag{28}$$

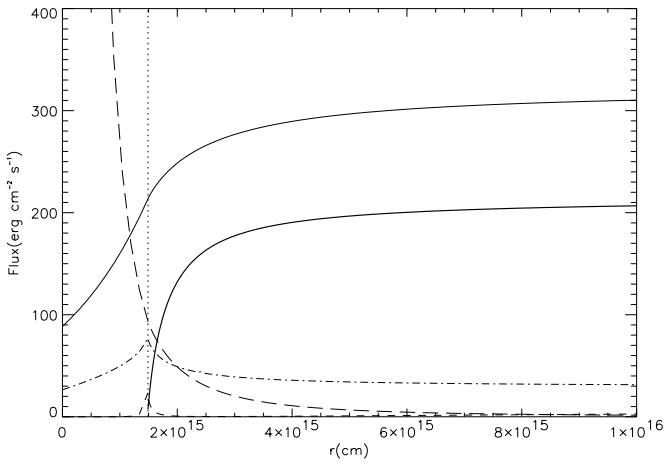

FIG. 6.—Flux density along the globule axis. The vertical dotted line indicates the position of the ionization front at $R_i = 100$ AU. The fluxes represented are nonionizing FUV radiation from θ^1 Ori C (*thin solid line*), ionizing EUV radiation from θ^1 Ori C (*thick solid line*), radiation from the globule central star (*long-dashed line*), recombination line radiation from the nebular environment and from the ionization front (*dot-dashed line*), Lyα radiation from the nebular environment and from the ionization front (*short-dashed line*), this last close to zero and mostly visible with a peak at the ionization front.

where $F_{\rm REC}$ refers to the recombination radiation emitted at the ionization front and $\sigma_g = \pi a_g^2$ indicates the geometrical cross section of a typical grain of radius a_g. A similar equation holding for the ionized flow includes the EUV flux and, in our approximation, has the distance, r, as the only independent variable.

The dust temperature depends strongly on the assumed grain parameters. Following Natta & Panagia (1976), we may take for reference "type 1" grains with $a_g = a_1 = 0.1$ μm and emissivity efficiency in the infrared

$$Q(\nu) = \frac{2\pi a_1}{\lambda} , \tag{29}$$

and the smaller "type 2" grains with $a_g = a_2 = 0.02$ μm and emissivity efficiency

$$Q(\nu) = 7 \times 10^{-4} \frac{a_2}{\lambda^2} . \tag{30}$$

Silicate features can be included by adding the spectral features provided by, e.g., Jäeger et al. (1994). Power-law emissivities allow analytical solutions to equation (28) for T_d. Writing the last two equations as

$$Q(\nu) = Q_0 \lambda^{-\beta} , \tag{31}$$

the blackbody-averaged dust opacity Q_β is

$$\begin{aligned} Q_\beta T_d^{4+\beta} &= \int_0^\infty Q(\nu)\pi B(\nu, T_d) d\nu \\ &= \begin{cases} 1.510 \times 10^{-4} Q_0 T_d^5 & \beta = 1 , \\ 5.150 \times 10^{-4} Q_0 T_d^6 & \beta = 2 . \end{cases} \end{aligned} \tag{32}$$

Equation (28) therefore becomes

$$T_d(r,\theta) = \left\{ \frac{[F_{\rm FUV}(r,\theta) + F_{{\rm Ly}\alpha}(r,\theta) + F_{\rm REC}(r,\theta)] + Q(\lambda_{T*}) F_*(r)}{4 Q_\beta} \right\}^{1/(4+\beta)} , \tag{33}$$

and a similar equation holds for the ionized wind. In Figure 7 we compare the temperature distributions along the globule axis resulting from the two types of grains, assuming the standard parameters. The smaller grains reach temperatures more than twice that of the larger grains, i.e., $T_d \simeq 260$ K versus $T_d \simeq 120$ K. Also, with the exception of the region closer to the central star ($r \lesssim 1/3 R_i$), the temperature is almost constant due to the weak dependency of the temperature on the flux. In the rest of this paper, we shall use type 1 grains to be consistent with our treatment of the disk, as also assumed by Chiang & Goldreich (1997, hereafter CG97). This choice allows us to use equation (33) to obtain the dust temperature and to apply the tabulated dust efficiency of Jäeger et al. (1994) to calculate a more realistic spectral energy distribution. We remark here that scattering of stellar radiation from dust grains is not considered in our model.

The emitted IR spectrum is given by the integrals

$$L_{\rm IR}(\nu) = \int_{R_0}^{R_i} \int_0^\pi \langle e^{-\tau(\nu)} \rangle n_d \pi a_g^2 Q(\nu) \pi B[\nu, T_d(r,\theta)] \times 2\pi r^2 \sin\theta d\theta \, dr \tag{34}$$

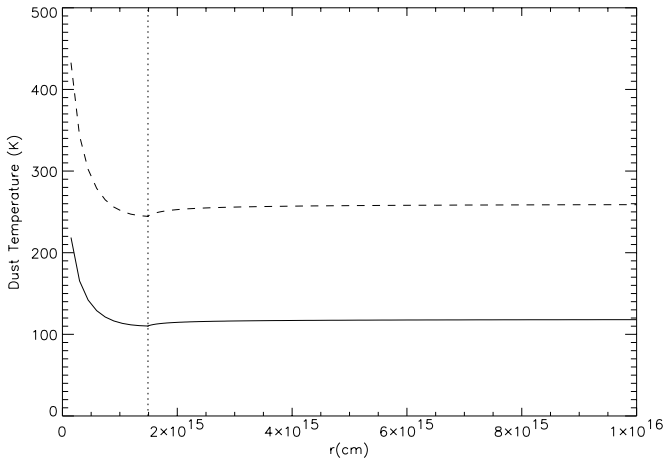

FIG. 7.—Temperature distribution along the globule axis resulting from the radiation sources represented in Fig. 6.

in the neutral part of the globule and

$$L_{\rm IR}(\nu) = \int_{R_i}^{R_\infty} \langle e^{-\tau(\nu)} \rangle n_d(r) \pi a_g^2 Q(\nu) \pi B[\nu, T_d(r)] \pi R_i^2 \, dr \tag{35}$$

for the ionized wind. To keep our treatment as simple as possible, we neglect the absorption of IR radiation in the energy budget of the envelope. This assumption is valid within the range of the optical depths in the UV and allows us to use equation (33) while avoiding the iterative computation of the IR radiative transfer. On the other hand, the 10 μm silicate feature can be self-absorbed even at our relatively modest optical depths, having an absorption cross section comparable to that at 2.2 μm. Therefore, we introduced the exponential factors in equations (34) and (35) to account for this effect.

Figure 8 shows the spectral energy distributions (SEDs), $\nu F_{\rm IR}(\nu)$, calculated for the Jäeger et al. (1994) dust grains and, for comparison, for the Panagia's type 2 grains. The resulting SEDs peak at $\approx$25 and $\approx$10 μm, respectively. Depending on the grain properties, the emission can be dominated by neutral globule or by the ionized shell.

4. EXTERNALLY ILLUMINATED DISKS

Our next step is to evaluate the IR SED of circumstellar disks embedded in H II regions. Although standard models for T Tauri disks assume the star+disk systems to be isolated, a number of studies have been devoted to the effects of the surrounding environment on the disk thermal structure and emitted spectrum. In particular, Natta (1993) and Butner, Natta, & Evans (1994) modeled the disks' thermal emission when they are surrounded by envelopes. Both studies find that at large distances from the central star the disks become significantly warmer than if direct heating alone was considered. The heating mostly affects the long wavelength emission from the disk. One may expect to obtain similar results for the disks in an H II region.

As for the globules, the disk temperature depends on a combination of heating by the central star in the disk, external heating due to the radiation directly coming from the ionizing star, and heating from the nebular environment.

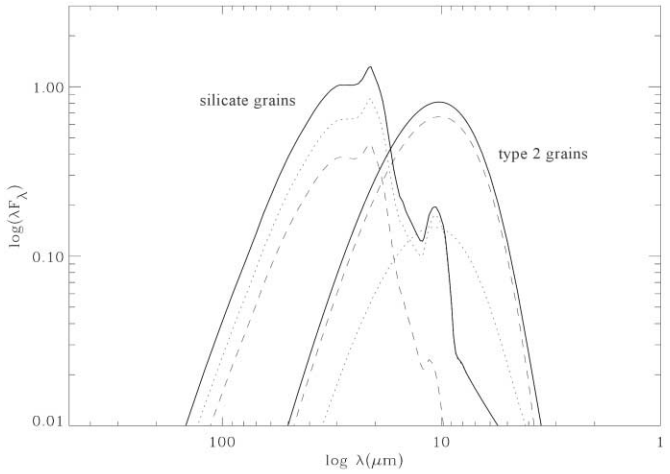

FIG. 8.—Spectrum emitted by a dusty globule with our standard set of parameters. The two solid curves are relative to type 1 grains (*left*) and type 2 grains (*right*). Each curve is the sum of the contributions from the neutral (*dashed line*) and ionized (*dotted line*) parts of the envelope. Self-absorption has not been considered. The stellar spectrum is not plotted.

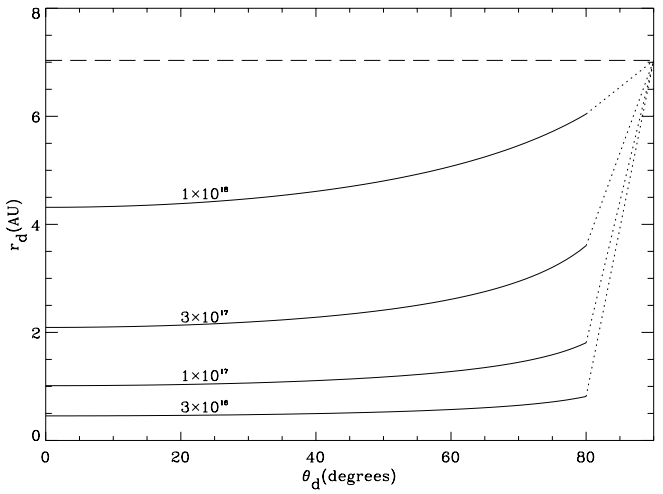

FIG. 9.—Radius a_d at which the disk heating from the central star equals that from the H II region as a function of the disk tilt angle θ_d and of the distance from θ^1 Ori C. From top to bottom, the lines represent decreasing distances from θ^1 Ori C. The dashed part of each line represents the case of pure nebular heating, occurring on the rear face of the disk (dark silhouette) within the H II region. The dotted lines at $\theta_d = 80°$–$90°$ are relative to the case of a disk aligned almost edge-on with respect to the direction of θ^1 Ori C. The stellar parameters are $T_* = 4500$ K and $L_* = 2.5\ L_\odot$.

We neglect heating from accretion, which should be a minor component outside a few stellar radii.

The radiation from the nebular environment typically hits the disk surface at angles much larger than α, the grazing angle of the radiation coming from the central star. In particular, the flux coming directly from the ionizing star depends on the tilt angle, θ_d, of the disk axis with respect to the direction of the ionizing source and acts only on one of the two disk faces. The nebular radiation, isotropic and roughly constant within the nebula, flows uniformly into the entire disk surface. For a geometrically thin, optically thick disk it is $\alpha \approx 0.4R_*/a$ (Ruden & Pollack 1991) and the energy input from the disk's central star will be dominant over the external radiation at disk radii

$$a_d \leq R_* \left[\frac{L_s}{4\pi d^2}\cos(\theta_d) + \frac{3\rho L_s}{16\pi R_{\rm H\,II}^2}\right]^{-1/3} \left(\frac{3\pi}{2\sigma T_*^4}\right)^{-1/3} \quad (36)$$

$$= 1.4\left(\frac{R_*}{R_\odot}\right)\left[\frac{\cos(\theta_d)}{d_{0.1}^2} + 0.26\right]^{-1/3}\left(\frac{T_*}{T_\odot}\right)^{4/3} \text{AU} \quad (37)$$

on the side facing the ionizing star, or

$$a_d \leq R_* \left(\frac{3\rho L_s}{4\pi R_{\rm H\,II}^2}\right)^{-1/3} \left(\frac{3\pi}{2\sigma T_*^4}\right)^{-1/3} \quad (38)$$

$$= 7.1\left(\frac{R_*}{R_\odot}\right)\left(\frac{T_*}{T_\odot}\right)^{4/3} \text{AU} \quad (39)$$

on the opposite face, having used the standard parameters and having indicated with $d_{0.1} = d(\text{pc})/0.1$ pc. In Figure 9 a_d is plotted as a function of the disk tilt angle θ_d for various distances from the ionizing star. The dashed line represents the limit of pure nebular illumination. This occurs (1) on the disk face opposite to the ionizing star and (*2*) on both faces if the disk is oriented edge-on with respect to the ionizing star ($\theta_d \simeq 90°$), and (3) at large distances from the ionizing star. Figure 9 clearly shows that, with our standard set of parameters, the heating of typical circumstellar disks is generally dominated by the nebular environment at distances larger than a few AU.

In reality, the EUV flux hardly reaches the disk surface in environments like the core of the Orion Nebula, since the neutral photoevaporated wind pushes away the ionization front from the disk. All radiation fields, including the radiation from the disk's central star, are attenuated by the evaporated wind. In the next section, devoted to the actual predictions for the SEDs of photoionized globules in the Orion Nebula, this effect will be explicitly taken into account. Here, however, we shall not reduce the external fluxes by generic absorption coefficients. This because, on the one hand, the main goal of this section is to illustrate how we build the model, and we want to keep the formalism as close as possible to our assumed reference model for circumstellar disks. On the other hand, at large distances from the ionizing star, photoevaporation can be so negligible that the diluted EUV flux can actually reach the disk surface. Prominent photoevaporated proplyds in the Orion Nebula are clearly concentrated within $\approx 30''$ from θ^1 Ori C. In particular, one does not expect the rear face of the disks to be photoevaporated, as it is heated only by the disk's central star and by the nebular radiation possibly attenuated by the evaporated material streaming away from the system (the cometary tails of the proplyd). The dark disks seen in silhouette against the nebular background do not show evidence for photoevaporeted winds (McCaughrean & Stauffer 1994). In principle, they can be modeled using the equations presented in this section. The reader is cautioned, in any case, that a comparison with real sources should take into account absorption effects.[3]

[3] For reference, the envelope discussed in the previous section reduces the flux from the ionizing star by a factor of $\approx\frac{1}{5}$, an amount comparable to moving the source twice as far.

4.1. *Disk Spectral Energy Distributions*

We calculate the disk emission using our modified version of the CG97 model, which provides a self-consistent treatment of the vertical hydrostatic equilibrium and radiative transfer of a disk. Disk flaring results from the hydrostatic equilibrium of the disk material in the gravitational field of the central star (Shakura & Sunyaev 1973; Kenyon & Hartmann 1987). In the CG97 model, radiation from the central star grazes the disk surface at an angle α and is entirely absorbed once it has reached a tangential optical depth $\tau_{\parallel} \simeq 1$ at the characteristic wavelength of the stellar radiation. This absorption produces an optically thin layer of "superheated" dust grains, since the grain emissivity in the infrared is lower than the absorption efficiency in the visible. Half of the radiation emitted by the layer goes inward and regulates the inner disk temperature.

We have modified this scheme to account for the external radiation field. Since the external radiation usually hits the disk at an angle much larger than α, photons entering along the normal to the disk surface will be absorbed deeper in the disk than those coming from the central star. We introduce a perpendicular optical depth $\tau_{\perp}$ related to the tangential optical depth by the equation $\tau_{\perp} \approx \tau_{\parallel}\alpha$. Instead of referring to the $\tau_{\parallel} = 1$ limit for the grazing radiation as CG97, we use the optical depth, $\tau_{\perp}$ as the variable that governs the propagation of the radiation through the disk. In this way, the dust temperature can be estimated at any disk radius, a, as a function of $\tau_{\perp}$ instead of the single value estimated at $\tau = 1$ by CG97.

With these assumptions, the flux from the central star is attenuated by a factor, $e^{-\tau_{\perp} Q(\lambda_{T_*})/\alpha(a)}$, within the disk, whereas the flux from the ionizing star is reduced by a factor, $e^{-\tau_{\perp}/\cos\theta_d}$. To be consistent with the notation used in the previous sections, $\tau_{\perp}$ is now the optical depth at UV wavelengths. In principle, the disk flaring produces a modulation of θ_d, but we ignore this effect considering that the variations average to zero over the circumference. We also assume that all the radiation coming from the ionizing star is locally absorbed by the dust, directly or through absorption of recombination radiation. It is, therefore,

$$F_d^s(\tau_{\perp}) = \frac{L_s}{4\pi d^2}\cos(\theta_d) e^{-\tau_{\perp}/\cos\theta_d} \, . \tag{40}$$

The attenuation of the nebular radiation within the disk can be readily expressed as a function of $\tau_{\perp}$ by using equation (16), assuming the disk curvature is negligible:

$$F_{\rm nebular}(\tau_{\perp}) = \frac{\rho L_s}{8\pi R_{\rm H\,II}^2}\left[\int_0^1 e^{-q\tau_{\perp}/x}\, dx + 2\int_0^1 e^{-\tau_{\perp}/x}\, dx\right] , \tag{41}$$

where x is the distance from the normal to the disk surface. The two terms on the right-hand side represent the Lyα and the nebular lines, respectively. The total external flux on the disk face pointing to the ionizing star is therefore

$$F_{\rm out}(\tau_{\perp}) = F_d^s(\tau_{\perp}) + F_{\rm nebular}(\tau_{\perp}) \, , \tag{42}$$

whereas on the other face only the term containing $F_{\rm nebular}(\tau_{\perp})$ will be present.

The external radiation affects the geometry of the disk. In particular, the grazing angle, $\alpha(a)$, depends on the external flux. Following CG97, it is

$$\alpha(a) \approx \frac{\alpha_1}{a} + a\frac{d}{da}\left(\frac{H}{a}\right) , \tag{43}$$

where $\alpha_1 \simeq 0.4\ R_*$ and H is the disk height above the midplane. For a disk vertically isothermal, it is

$$\frac{H}{a} \approx 4\left(\frac{a}{R_*}\right)^{2/7}\left(\frac{T_e}{T_c}\right)^{4/7} , \tag{44}$$

where the effective temperature, T_e, is a measure of the energy input at the disk surface and $T_c = GM_*\mu/(kR_*)$, μ being the mean molecular weight of the gas. If an outer radiation field is present, it is

$$T_e(a) \approx \left[\left(\frac{\alpha}{2}\right)\left(\frac{R_*}{a}\right)^2 T_*^2 + \frac{F_{\rm out}(0)}{\sigma}\right]^{1/4} . \tag{45}$$

With this expression for T_e, equation (43) cannot be solved analytically. In the limit of outer radiation field dominating the disk heating (i.e., at large distances from the disk central star), the first term can be neglected and we have

$$\frac{H}{a} \approx 4\left(\frac{a}{R_*}\right)^{1/2}\left\{\frac{[F_{\rm out}(0)/\sigma]^{1/4}}{T_c}\right\}^{1/2} . \tag{46}$$

In this case,

$$\alpha(a) \approx \frac{\alpha_1}{a} + \alpha_3 a^{1/2} \, , \tag{47}$$

with

$$\alpha_3 = 2\left\{\left[\frac{F_{\rm out}(0)}{\sigma}\right]^{1/4}\frac{1}{T_c R_*}\right\}^{1/2} . \tag{48}$$

In Figure 10 we show the vertical disk profiles calculated for a disk facing the ionizing star at $d = 0.1$ pc, with no extinction in front of the disk surface. In this situation, the flaring calculated on both faces, i.e., with and without the EUV radiation, is significantly higher than that resulting from the standard CG97 model. In practice, these disk profiles are indicative only of an optical depth surface, since when photoevaporation is present there is no discontinuity between the disk surface and the envelope. A large flaring angle can rather be regarded as an indication for disk photoevaporation. The case with no direct radiation from the ionizing star provides the minimum flaring profile for the back surface of a disk within the H II region (assuming negligible extinction from the envelope material).

The disk flaring will be dominated by the external flux at distances larger than

$$R_{\rm flaring} = \left(\frac{4}{7}\right)^{14/3} T_*^{8/3} T_c^{-1/3}\left(\frac{F_{\rm out}}{\sigma}\right)^{-7/12} R_* \, . \tag{49}$$

With our typical parameters, $R_{\rm flaring} \simeq 2$ AU.

The temperature of the superheated dust layer is given by the combination of internal and external contributions at

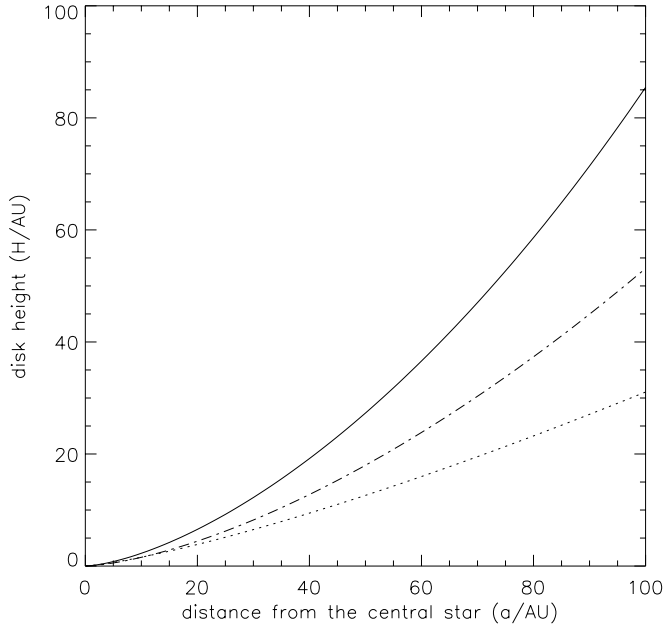

FIG. 10.—Vertical sections of the disk. The continuous line represents the locus of the disk photosphere when both the flux from θ^1 Ori C and the nebular radiation are taken into account. The dot-dashed line has been obtained by neglecting the flux from θ^1 Ori C and is therefore representative of the dark face of the disk. The dotted line has been obtained taking into account only the radiation from the disk central star (as in CG97).

the optical depth, $\tau_\perp$:

$$T_{ds}(\tau_\perp, a) = \left[\left(\frac{R_*}{a}\right)^2 \sigma T_*^4 e^{-\tau_\perp Q(\lambda_{T_*})/\alpha(a)} + \frac{2}{\alpha(a)} F_{\rm out}(\tau_\perp)\right]^{1/(4+\beta)} \left(\frac{T_{d1}^\beta}{2\sigma}\right)^{1/(4+\beta)}, \quad (50)$$

where

$$T_{d1} = \frac{hc}{8\pi a_g k} \quad (51)$$

is a characteristic temperature of the dust grains, related to the blackbody-averaged dust emissivity at temperature T by

$$\bar{Q}(T) = \left(\frac{T}{T_{d1}}\right)^\beta . \quad (52)$$

In Figure 11 we plot the temperature distribution calculated at various distances from the central star as a function of the vertical optical depth. By comparison, the CG97 approximation of uniform temperature across the superheated layer,

$$T_{ds} = \left[\left(\frac{R_*}{a}\right)^2 \sigma T_*^2 + F_{\rm out}(0)\right]^{1/(4+\beta)} \left(\frac{T_{d1}}{4\sigma}\right)^{1/(4+\beta)}, \quad (53)$$

would have provided $T_{ds} = 355$, 220, 147, and 113 K for the $a = 3$, 10, 30, and 100 AU, respectively.

The flux emitted by the superheated layer will be given by

$$F(a,\nu) = \int_0^3 e^{-\tau'_\perp Q(\nu)} Q(\nu) B_\nu\left[\nu, T_{ds}(\tau'_\perp, a)\right] d\tau'_\perp \quad (54)$$

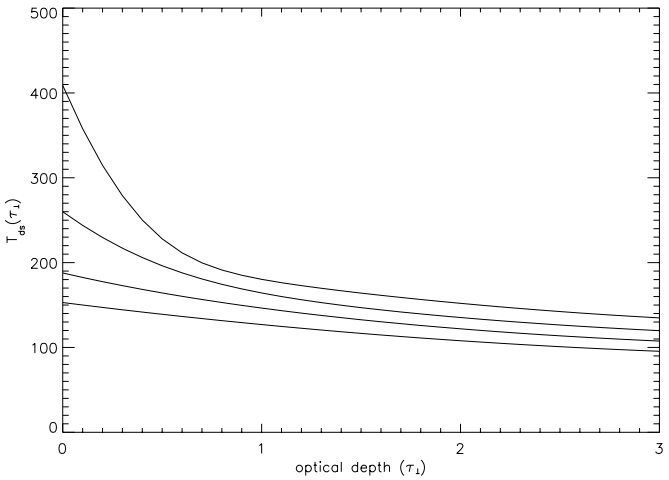

FIG. 11.—Temperature of the superheated layer in absence of external luminosity at distances (*top to bottom*) $a = 3$, 10, 30, and 100 AU from the central star.

having assumed that all the flux is absorbed when $\tau_\perp = 3$. The luminosity density from the superheated layer, normalized to the stellar luminosity L_*, is

$$L_{ds}(\nu) = \frac{8\pi^2\nu}{L_*}\frac{1}{2}\int_{a_i}^{a_o} F(a,\nu) da , \quad (55)$$

where $a_i = 0.07$ AU and $a_o = 100$ AU are our assumed inner and outer disk radii, and we have taken into account that only half of the flux is radiated in the outer space.

In what concerns the inner disk, we adopt the same scheme of CG97 with modifications needed to account for the ambient radiation. Equations (12a)–(12c) of GC97 now become

$$T_{\rm in}(a) \approx \frac{1}{2^{1/4}}\left[c_4^4 a^{-3/2} + \frac{F_{\rm out}(0)}{\sigma}\right]^{1/4} \quad \text{(region A)},$$

$$T_{\rm in}(a) \approx \frac{T_{d1}^{\beta/(4+\beta)}}{(2K_V\Sigma_0)^{1/(4+\beta)}}\left[c_4^4 + \frac{F_{\rm out}(0)}{\sigma} a^{3/2}\right]^{1/(4+\beta)} \quad \text{(region B)},$$

$$T_{\rm in}(a) \approx \frac{1}{2^{1/(4+\beta)}}\left[c_4^4 a^{-3/2} + \frac{F_{\rm out}(0)}{\sigma}\right] \times \left[\left(\frac{R_*}{a}\right)^2 \sigma T_*^4 + \frac{F_{\rm out}(0)}{\sigma}\right]^{1/(4+\beta)} T_{ds}^{1/(4+\beta)} \quad \text{(region C)}. \quad (56)$$

having defined c_4 as

$$c_4 = \left(\frac{\alpha_3}{4}\right)^{1/4} R_*^{1/2} T_* . \quad (57)$$

The three regions are limited by the radii $a_{a|b}$ and $a_{b|c}$, derived by setting $\tau_\perp \cong 2$ and $\tau_\perp \cong 1.5$, respectively. With CG97, we have defined

$$\tau(a) = \bar{Q}_{1,2}\kappa_V \Sigma_0 a^{-3/2} , \quad (58)$$

with $\bar{Q}_1 = (T_{\rm int}/T_{d1})^\beta$ and $\bar{Q}_2 = (T_{ds}/T_{d1})^\beta$ for the two conditions, $\kappa_V = 400$ cm^2 g^{-1} and $\Sigma_0 = 10^3$ g cm^{-2}. Consistent with CG97, we used equation (53) for the temperature, T_{ds}.

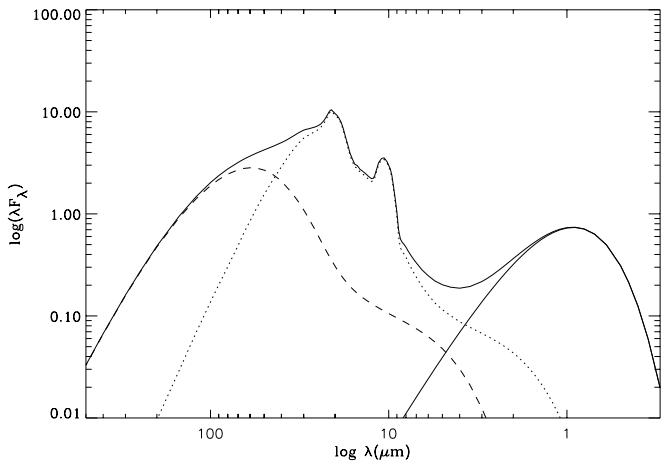

FIG. 12.—SED for a hydrostatic, radiative equilibrium disk directly exposed to the flux from θ^1 Ori C. *Solid line:* stellar photosphere; *dotted line:* superheated layer; *dashed line:* inner disk. The thick solid line represents the total SED. The standard set of parameters with Jäeger et al. (1994) silicates has been assumed.

With our standard parameters, $a_{a|b} = 140$ AU. The temperature of the internal disk is constant at $T_{d1} \simeq 60$ K over most of the disk. The luminosity density from the disk interior normalized to the stellar luminosity $L*$ is now

$$L_{\rm in}(\nu) = \frac{8\pi^2\nu}{L*} \int_{a_i}^{a_o} \left[1 - e^{-\tau_\perp(x,\nu)}\right] B[\nu, T_{\rm in}(x)] x\, dx\ . \quad (59)$$

Figure 12 shows the SED for the front surface of the flared disk. The distribution reaches a minimum at ≈ 4 μm and then rises up to a maximum at ≈ 60 μm. The silicate peaks prominent at 10 and 20 μm are emitted in the superheated layer. In Figure 13 we present the SED for the face of the disk opposite to the ionizing star. There is a general reduction of the disk luminosity, both from the superheated atmosphere at short wavelengths and from the interior in the far-IR. As we already mentioned, this type of SED can be representative of the dark silhouettes seen in projection against the nebular background in Orion. For these disks, Lyα radiation may play a role only if the disks are still embedded within the H II region, whereas the other nebular radiation is relevant also if the disk is in the PDR region behind the ionization front. One must remember that the Orion Nebula is essentially density-bounded in the direction of the Earth, being limited by a nonuniform veil of foreground material that is not completely optically thick (O'Dell & Yusuf-Zadeh 2000). Dark silhouette disks can therefore be subject to a broad range of radiative input, as shown for example by the presence of [O I] emission in only one object reported by Bally et al. (2000).

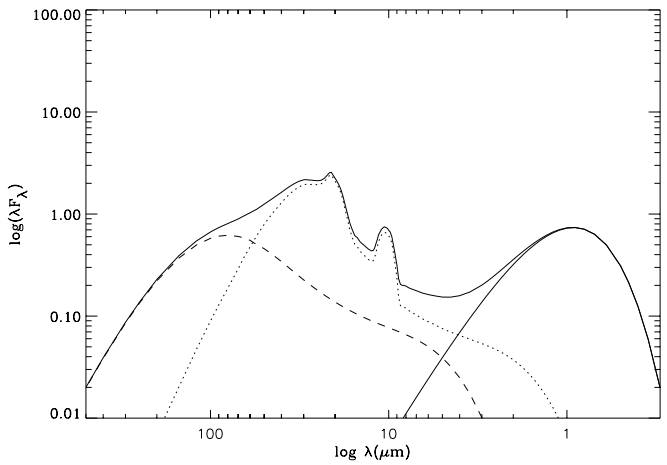

FIG. 13.—Same as Fig. 12, for a hydrostatic, radiative equilibrium disk directly exposed to the nebular radiation only.

5. PHOTOIONIZED PROPLYDS

In this section, we model the thermal emission produced by a photoevaporated disk enshrouded in a dusty photoevaporated envelope. We treat the envelope as a dusty photoionized globule of the type discussed in § 3, whereas the disk treatment will follow the model presented in the previous section. However, when the globule is merged with the disk, some of the assumptions adopted for the isolated cases are no longer valid:

1. The disk is now directly exposed to only a fraction of the outer radiation, owing to the globule attenuation. In particular, no EUV radiation reaches the surface of the disk.
2. The disk is exposed to the radiation reemitted by the globule, mostly in the infrared. We shall assume that the IR radiation crosses undisturbed the superheated layer and is absorbed in the inner disk.
3. The feedback contribution of the disk emission to the heating of the globule can be neglected, since a passive disk emits mostly in the far-IR, where the dust opacity is negligible.
4. The radiation emitted by the disk and by the central star is attenuated crossing the envelope. We also take into account the attenuation of the envelope radiation within the envelope itself.

We shall assume the globule to be spherical with the disk lying in the equatorial plane. Both angles θ_d, between the disk axis and the direction of the ionizing star, and $\theta_\oplus$, between the disk axis and the Earth are critical to model SEDs matching the observational data. They have been taken into account in an approximate way: the former modulates the amount of stellar radiation falling on the disk surface through equation (40) but not on the envelope. The latter affects the tilt angle of the disk with respect to the observer. For simplicity, however, the plots presented in this section have been obtained assuming both $\theta_d = 0°$ and $\theta_\oplus = 0°$. A disk oriented face-on both to the ionizing star and to the Earth is located along the line of sight of, and behind, the ionizing star.

The globule structure is described by the same set of equations discussed in § (3). The only change is that the term containing I_ν^2 in equation (22) is now equal to zero, since the disk, optically thick to ultraviolet radiation, shields the hemisphere opposite to the ionizing star. In what concerns the radiation flowing into the disk, both the fluxes coming from the H II region and from the central star are attenuated by the globule. In agreement with our previous assumption of FUV dominated flows, the EUV flux is entirely absorbed before reaching the surface of the disk. The radiation propagates through the superheated layer and then through the disk interior. Only the IR flux reemitted by the globule crosses the thin layer undisturbed.

The total IR flux emitted by the globule and reaching the disk surface is given by

$$F(a) = \int_0^{2\pi} \int_0^{\theta_{\max}(a)} \int_{R_i}^{R_\infty} \int_0^{\infty} \frac{F_{\rm env}(r,\theta,\phi,\nu)}{4\pi d_a^2} \times \cos\theta_a r \sin\theta \, d\nu \, dr \, d\theta \, d\phi \, , \quad (60)$$

where $F_{\rm env} = n_d \pi a_g^2(\nu) B(\nu, T_d)$ is the flux emitted by a cubic centimeter of dust within the globule (see eqs. [34] and [35]), and d_a is the distance between the point, $P(r,\theta,\phi)$, within the envelope and a point, A, on the surface of the disk at a projected (equatorial) distance, a, form the star and on the plane defined by $\phi = 0$. It is

$$d_a = \left[r^2 + (2a\sin\theta\cos\phi - \cos\theta\tan\alpha)r + a^2(1+\tan\alpha)\right]^{1/2} , \quad (61)$$

and θ_a is the angle between the line, PA, and the normal to the disk surface, given by

$$\theta_a = \sin\alpha \frac{r\sin\theta\cos\phi}{d_a} + \cos\alpha \frac{r\cos\theta - a\tan\alpha}{d_a} \, . \quad (62)$$

An accurate estimate of d_a would require an iterative solution of equation (60), since the actual position of the point, A, within the globule depends on the flaring angle, $\alpha(a)$, which in turn depends on the radiative heating on the disk. To avoid the rather heavy numerical computation, we adopted the approximate assumption that the position of point, A, is initially given by equation (47), this time with the absorption through the envelope explicitly taken into account, and then used the value of $F(a)$ resulting from equation (60) to recalculate the disk flaring angle.

The flux emitted by the disk is calculated following the treatment presented in § 4 with a few changes. We assume that the temperature of the superheated layer does not depend on the flux emitted by the globule, as the IR emission propagates almost undisturbed through the disk atmosphere. Owing to presence of the absorbing envelope, the flaring angle now depends on the distance, a, also via the external flux, $F_{\rm out}$ (eq. [42]). In general, $R_{\rm flaring}$ (eq. [49]) remains of the order of a few astronomical units over a broad range of parameters, and even when the extinction by the wind/envelope is included, as it affects both the flux from the disk central star and from the outer space. Within the Orion Nebula the disk flaring is usually dominated by the external flux, so we shall adopt the approximation of equation (47). The luminosity of the superheated layer is given by equations (54) and (55). In what concerns the temperature of the disk interior, it will depend on the sum of the IR radiation received from the superheated layer and from the globule, plus the flux emitted by the disk interior itself when the disk is optically thick. Equations (56)–(59) apply also in this case.

Neglecting the interstellar contribution, the optical depth between P and an observer on the Earth is

$$\tau_\nu(r,\phi,\theta,\theta_\oplus) = \tau_{R_i} Q(\nu) \left[\left(\frac{r}{R_i}\sin\theta\cos\phi + \sin\theta_R\cos\phi_R \right)^2 + \left(\cos\theta_R - \frac{r}{R_i}\cos\theta \right)^2 \right] . \quad (63)$$

The angles, θ_R, and, ϕ_R, define the point where the line from P with angle, $\theta_\oplus$, intercepts the globule surface. They are related to the coordinates of P and to $\theta_\oplus$ by the equations

$$r\sin\theta\sin\phi = R_i \sin\theta_R \sin(\pi - \phi_R) \quad (64)$$

and

$$\tan\theta_\oplus = \frac{r\sin\theta\cos\phi + R_i\sin\theta_R\cos(\pi-\phi_R)}{R_i\cos\theta_R - r\cos\theta} \, , \quad (65)$$

solved numerically. Crossing the ionized wind, the radiation is further attenuated by an optical depth $\simeq Q_\nu \tau_d^\infty$. We neglect the self absorption of the IR radiation emitted by the ionized wind

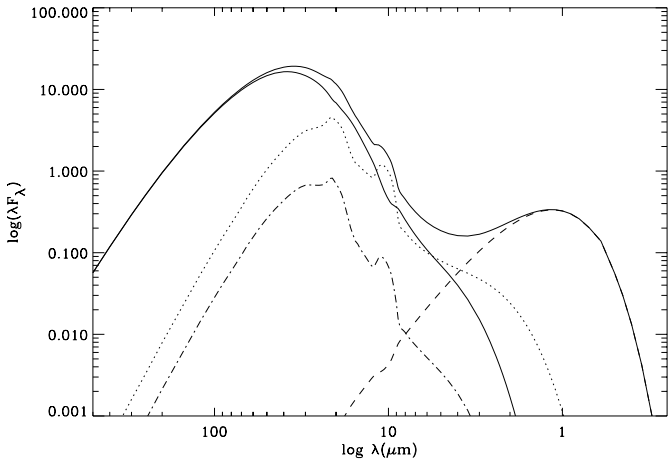

FIG. 14.—SED of a flaring disk embedded within a photoevaporated envelope. *Solid line:* stellar photosphere; *dotted line:* superheated layer; *dashed line:* inner disk; *dot-dashed line:* outer envelope; *thick solid line:* total SED.

Figure 14 shows the SED distribution arising from the front face of the disk. With our standard set of parameters, the emission is dominated by the disk atmosphere at wavelengths $\lesssim 40$ μm and by the internal disk emission at longer wavelengths. The envelope emission never produces a noticeable contribution. The disk atmosphere has a pronounced peak of emission at 3 μm due to secondary heating by the envelope. The relevance of this effect depends on the amount of dust located in the immediate surroundings of the star. We have assumed uniform density within the globule up to the dust evaporation radius, which is of the order of a few stellar radii. A larger dust free cavity would significantly reduce the intensity of the 3 μm bump.

6. DISCUSSION

The geometry we have assumed to illustrate the physical basis of our model represents in practice an extreme case. A disk oriented face-on with respect to the ionizing star receives the maximum amount of radiation. This causes a substantial increase of the flaring angle and therefore of the inner stellar flux intercepted by the disk. If the disk is also oriented face-on with respect to the Earth, the observer will receive the highest amount of disk radiation. Even if chances of having such a fortunate alignment are rather low, one of the most intriguing 10 μm sources of the Orion Nebula, SC3 (McCaughrean & Gezari 1991; Hayward et al. 1994; Fig. 15) can be readily interpreted in this way. With a 10 μm flux of $\simeq$4 Jy, SC3 is the brightest compact source in the

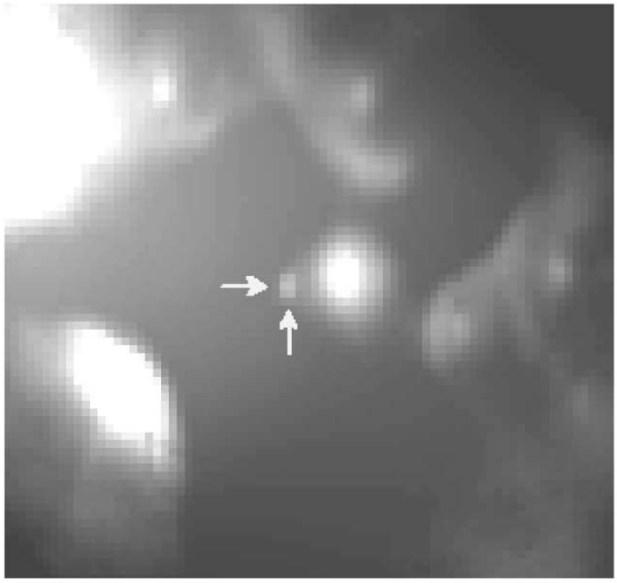

FIG. 15.—Image at 10 μm of the θ^1 Ori C field. The arrows mark the position of θ^1 Ori C. Source SC3 is the bright knot at located $\approx 1''$ to the west of θ^1 Ori C. The field size is approximately $15'' \times 15''$ and the pixel size is $0''.26$ pixel^{-1}. The image has been obtained with the MAX camera on UKIRT and is part of a large mosaic of the Orion Nebula core (M. Robberto et al. 2002, in preparation).

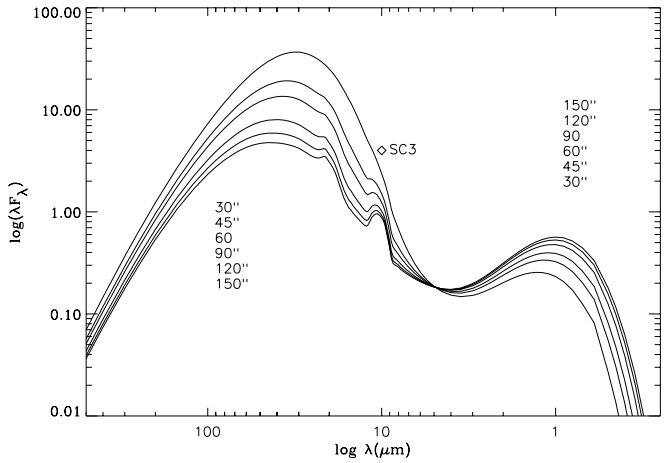

FIG. 16.—SED of a flaring disk embedded within a photoevaporated envelope for different values of the distance from θ^1 Ori C. The thick line refers to the standard case.

Orion Nebula, excepting the BN/KL region. It is located at a projected distance $\approx 1''$ west of θ^1 Ori C, and mostly for this reason it has never been observed at wavelengths shorter than 2 μm. In our 10 μm images, SC3 is spatially resolved with FWHM $\simeq 0''.5$, corresponding to approximately 200 AU, the typical size of circumstellar disks in Orion. A direct comparison with the nearby complex of arclike structures produced by the wind-wind interactions suggests that SC3 is a different kind of phenomenon. Despite the fact that it has the shortest projected distance from θ^1 Ori C, SC3 is apparently undisturbed by the powerful wind from the O6.5 star, as it is the only extended source with circular shape. This indicates that the physical distance between SC3 and θ^1 Ori C is much larger than for the other sources. The simplest interpretation is that SC3 is a star+disk system in the background with respect to θ^1 Ori C with a very high mid-IR brightness produced by the disk being oriented face-on both to θ^1 Ori C and to us. Figure 16 shows that the 10 μm photometry of SC3 is compatible with our standard model and a distance slightly lower than $30'' = 0.065$ pc. It must also be noticed that the low-resolution 10 μm spectrum of SC3 obtained by Hayward et al. (1994) shows silicate emission, whereas our standard model predicts at these distances an almost featureless SED dominated by the inner disk emission. Further data on this sources are needed to constrain our set of parameters.

In general, disks are randomly tilted with respect both to the ionizing star and to the Earth, and therefore their apparent brightness will be reduced in comparison to our standard case. In § 4.1 we stated that the tilt angle with respect to the ionizing star, θ_d, can be simply accounted for by a projection factor $\cos\theta_d$ in the flux received by the disk surface. However, this is strictly true only for tilt angles $\theta_d < \alpha(a_o)$. Since disks are intrinsically flared, large tilt angles may cause part of the surface exposed to the ionizing star to go under the edge's shadow. When this happens, the heating of the surface is no longer uniform, the flaring angle varies with the azimuthal angle, and the disk loses its symmetry around the rotation axis. Along its orbit around the central star, the disk material will experience a periodic modulation of pressure and temperature, and the resulting differential drag may cause the disk to warp. Photoevaporation will occur only from the area directly exposed to the flux from the ionizing star, as well as on the opposite disk edge. Photoevaporation from the edge appears compatible with the observations showing that disks in the Orion Nebula are truncated (McCaughrean, Stapelfeldt, & Close 2000). As the analysis of the structure and evolution of circumstellar disks in these conditions goes beyond the scope of this paper, one can maintain the "$\cos\theta_d$" treatment to account for a reduced flux falling on the disk surface, keeping in mind that the derived tilt angle in this case is an overestimate of the real one.

In what concerns the tilt angle with respect to the Earth, $\theta_\oplus$, Chiang & Goldreich (1999) have studied the corresponding variation of the SEDs for isolated disks. They found that the SED shows negligible variations until $\theta_\oplus$ approaches the flaring angle at the disk outer radius $\alpha(a_o)$. When the inner disk regions enter in the shadow, the short-wavelength emission begins to disappear from the vantage point of the observer. To account for this effect, we simply multiply the flux emitted by the disk at each radius by the fraction of visible area. Figure 17 shows the dramatic reduction of the disk brightness at short wavelengths, together with the stellar radiation, when $\theta_\oplus$ increases from 45° to 50° crossing $\alpha(a_o) \simeq 48°$. Our geometrical treatment is valid only as long as the disk is optically thick at all wavelengths and large enough to contain a strongly flared surface. In the scheme of CG97, the outer disk regions are in a completely optically thin regime (region C of eq. [56]), and therefore the transition is modulated by the variation of optical depth across the disk. In our case, however, the truncated disk remains optically thick (region A) up to the disk edges. We find that the disk remains optically thick up to $a_o \simeq 100$ AU over a wide range of parameters. In particular, our standard disk+envelope model has $a_{a|b} = 113$ AU. Thus, the change of SED at short wavelengths is much more abrupt. The decrease of disk emission at $\lambda > 30$ μm is correct as long as

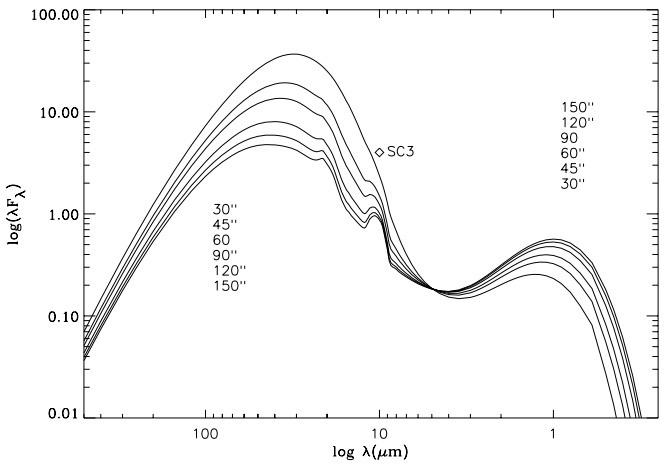

FIG. 17.—SED of a flaring disk embedded within a photoevaporated envelope for different values of the tilt angle with respect to the Earth $\theta_{\oplus}$. The thick line refers to the standard case.

the outer parts of the disk are also optically thick and, therefore, sensitive to the disk orientation. In conclusion, the disk orientation with respect to the Earth can be regarded as like a " switch " for the short-wavelength radiation. If the star is directly visible (e.g., with the *Hubble Space Telescope* [*HST*]), then the brightness at near- and mid-IR wavelengths will be high; otherwise if the star is invisible. Transition objects with heavily reddened stars should be rare. Observations at 10 μm of dark silhouette disks appear to confirm this result: the large dark silhouette 114-426, seen edge-on, has a star under $A_v \geq 60$ mag of extinction (McCaughrean et al 1998) and remained undetected at $[N] \simeq 9$ in our deep survey performed with the UKIRT 3.8 m telescope (M. Robberto, S. V. W. Beckwith, & T. M. Herbst 2002, in preparation), whereas the dark silhouette with the brightest central star, object 218−354, has been detected at 10 μm both by Hayward & McCaughrean (1997) and by us.

In the standard case, the envelope contribution is negligible at all wavelengths with respect to that coming from the disk. For some disk orientations, however, the envelope emission becomes important. This because the envelopes are extended, and the larger the value of $\theta_{\oplus}$, the more the disk emission will be suppressed, whereas the fraction of envelope obscured by the disk will be negligible. If the disk is seen close to edge-on, the envelope emission may eventually dominate. Figure 18 shows two of the most prominent objects, sources 177-341 (HST 1) and 182-413 (HST 10), as observed by with MAX on UKIRT and, for comparison, with the *HST*. These systems, with the disks seen edge-on, are clearly resolved at 10 μm with some evidence of a central peak. Size and orientation in the mid-IR correspond to that observed in the recombination lines. These images provide conclusive evidence that photoevaporated dust can be heated in the photoionized globule and emit significantly in

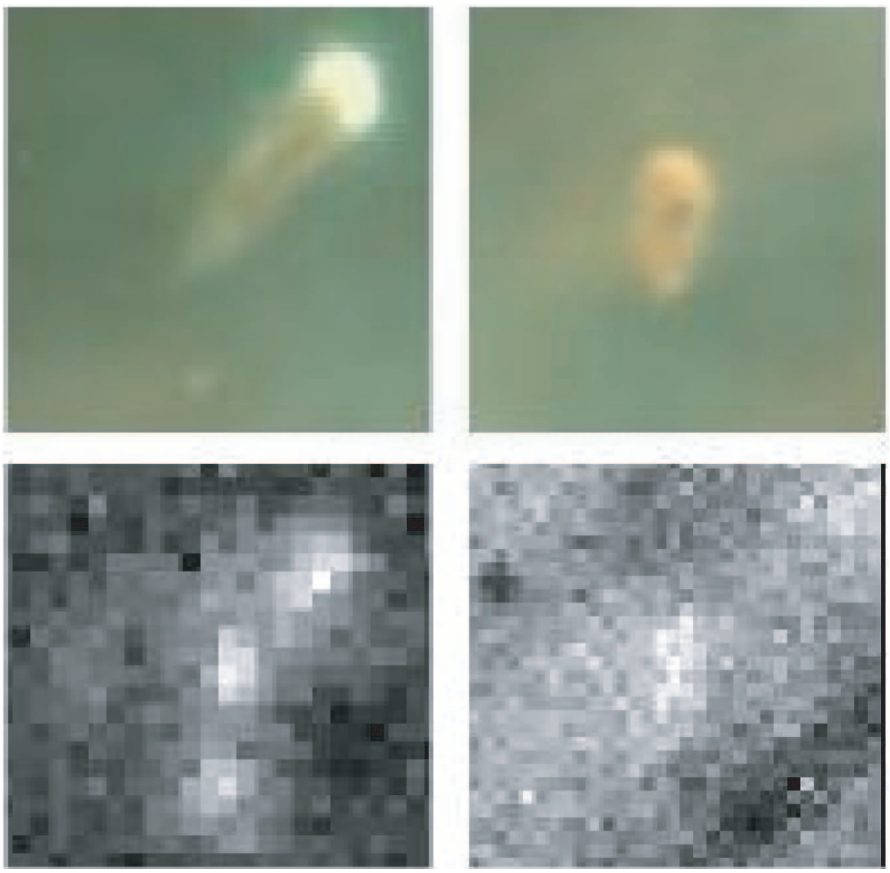

FIG. 18.—Prominent proplyd sources 177-341 (HST 1; *left*) and 182−413 (HST 10; *right*) imaged by the *HST* (*top*) and MAX on UKIRT (*bottom*). *HST* images refer to a combination of recombination lines, namely, [N II] (*red*), Hα (*green*), and [O III] (*blue*). The MAX images have been taken in *N* broadband with integration time of the order of 600 s on source (see M. Robberto et al. 2002, in preparation, for details).

the mid-IR, with brightness comparable to that of the disk. It is clear that all possible combinations of angles θ_d and $\theta_\oplus$ may generate a variety of SEDs similar to those presented in Figure 17. All are characterized by an SED peaking at $\simeq$30–60 μm and relatively low fluxes at wavelengths shorter than 10 μm.

Let us consider the impact of other basic parameters on the SEDs. In Figure 16 we present the SED obtained by placing our standard proplyd at various distances between 30″ ($d = 0.065$ pc) and 150″ ($d = 0.33$ pc) from the ionizing star. The SEDs are renormalized to the total stellar luminosity to compare their structure independently of the geometrical dilution of the signal with the distance. Still, the (relative) stellar flux in the visible increases with the distance, owing to the corresponding reduction of optical depth within the globule described in § 3.2 (see also Fig. 1). In the far-IR the flux drops with the distance because the outer disk is colder, as it receives less flux from the ionizing star, and it is therefore flatter, receiving less flux also from the central star. In comparison, the flux from the superheated layer is less affected by the distance from the ionionzing star, and for this reason the silicate peak in emission becomes relatively more prominent.

Figure 19 shows the variation of the SED with $R_{\rm out}$, the distance of the ionization front. We have considered $R_{\rm out} = 100$, 200, and 300 AU. The emerging stellar flux is reduced owing to the increase of optical depth in the envelope with the globule size (see again Fig. 1). The relative importance of the envelope emission increases significantly, but the SED is still dominated by the disk emission owing to the special alignment of our standard case mentioned above. To facilitate the comparison with our standard case, we have neglected here the contribution from the hemisphere opposite to the ionizing star.

The change of SED with the inner disk radius, a_i, is shown in Figure 20. The gap in the inner disk produces the expected decrease of the SED between 2 and 10 μm. Finally, the variation of SEDs with the stellar temperature is illustrated in Figure 21. Since we have kept the stellar radius constant, this plot also illustrates the variation of SEDs with the luminosity of the central star. Reducing the stellar temperature the disk emission becomes more and more important because the external contribution has been assumed to remain constant.

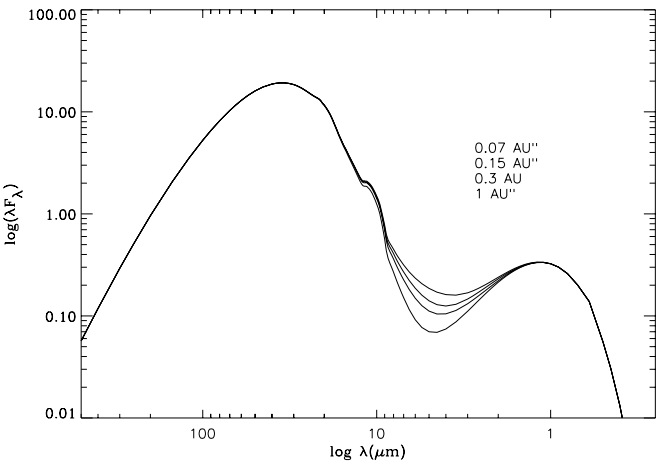

FIG. 20.—SED of a flaring disk embedded within a photoevaporated envelope for different values of the disk inner radius a_i.

A direct application of our model is presented in Figure 22, showing a fit to the available photometric data of source 177-341 = HST 1 (see Fig. 18). We have assumed $\theta_d = 45°$ and $\theta_\oplus = 75°$, to account for a disk seen nearly edge-on. We used a distance $d = 43\farcs2$, twice the projected distance from θ^1 Ori C. Hillenbrand (1997) gives a spectral type later than K6. We have adopted a $M1$ spectral type with $T_* = 3750$ K and radius $R_* = 2.18\ R_\odot$. Concerning the geometry, we have assumed an ionization front at $R_{\rm out} = 300$ AU and a disk with an inner radius $a_i = 0.3$ AU. To match the stellar photometry, we assumed $A_v = 2.2$. The model predicts $\tau_R = 1.45$, so that approximately 0.6 mag of visual extinction must be attributed to foreground extinction. In this fit, the envelope and disk have comparable brightness, the disk emission been provided by the disk interior.

Given the number of parameters left unconstrained by the available observational data, it is not surprising that with our model we are able to fit a single photometric point at 10 μm. On the other hand, the 10 μm photometry cannot be readily explained with conventional disk models. Our

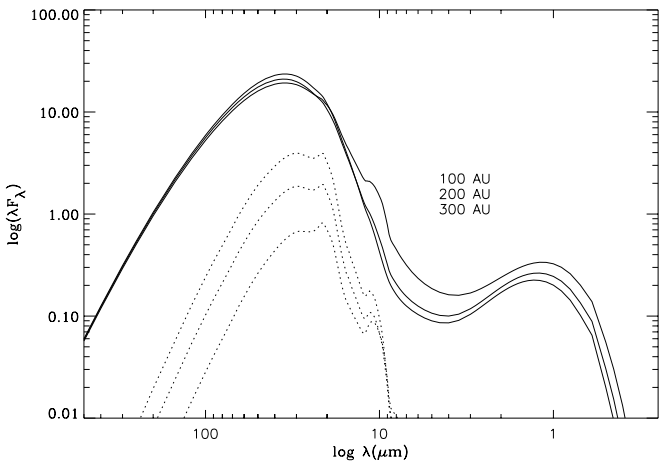

FIG. 19.—SED of a flaring disk embedded within a photoevaporated envelope for different values of the ionization radius $R_{\rm out}$.

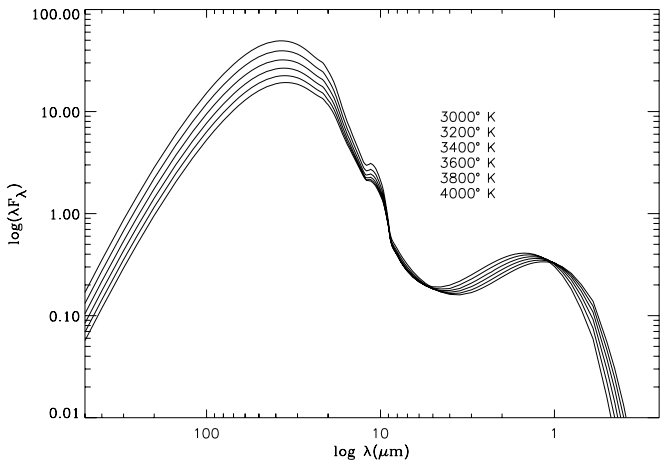

FIG. 21.—SED of a flaring disk embedded within a photoevaporated envelope for different values of the effective stellar temperature T_*.

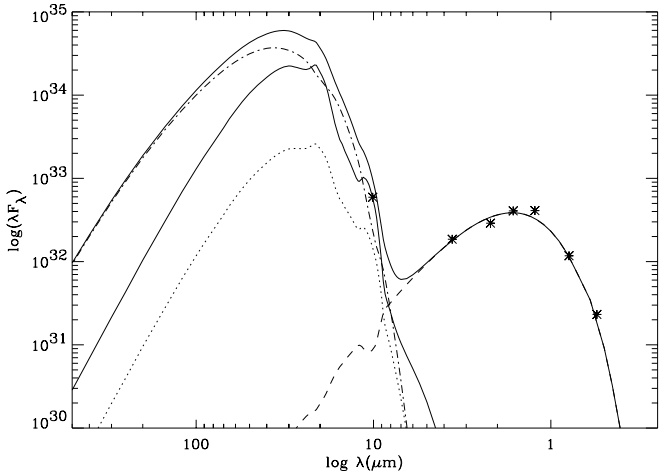

FIG. 22.—Photometry of the proplyd source 177-341 = HST 1 (*asterisks*) and model SED assuming a flaring disk embedded within a photoevaporated envelope. See text for the fit parameters. The 10 μm photometric point derives from the image presented in Fig. 18. Photometry at shorter wavelengths is from Hillenbrand (1997) and from Robberto et al. (2002, in preparation).

model also provides a strong prediction for high mid- and far-IR fluxes from these systems. Future high spatial resolution observations at these wavelengths will asses the validity of our assumptions and provide insights into the evolution of circumstellar disks in the most typical environmental conditions.

A number of assumptions deserve some additional comment. First, we have assumed that the disk atmosphere remains well defined and treatable by the CG97 approximation even when the flaring angles become extreme (up to $\simeq 45^{\circ}$). In presence of photoevaporation, however, the conditions of hydrostatic equilibrium used to set the disk profile are no longer valid, and the locus of the disk "atmosphere" should be recalculated taking into account the radially diverging flow. Second, although we have a basic understanding of the globule physics, it is still very hard to constrain the actual structure from the observations, deriving information such as the density distribution. Third, the grain properties are critical, not only in what concerns the absorption efficiencies (§ 3.4), but also the albedo, that we neglected. Scattering processes affect the near- and mid-IR emission of disks seen nearly edge on. Also, it has been shown that dust scattering in an optically thin envelope can contribute to the increase of disk temperature at large distances from the central star (Natta 1993), therefore adding a further contribution to the energy input at the origin of the disk flaring. Finally, we assumed in § 2 a simplified model for the Orion Nebula. It is known (O'Dell 2001a, 2001b) that the density in the Orion Nebula decreases with the distance from the interface with the Orion molecular cloud, where the main ionization front is located. Also, θ^1 Ori C is approximately 3 times closer to the main ionization front than to the foreground veil of neutral material, where a secondary ionization front is also located. The major effect of a more refined description would be a reduction of our estimates for the Lyα energy density. We have seen that this is a secondary source of dust heating. A modulation over the r^{-2} dependency of the central radiation field would also be introduced. This effect may be significant in future studies aimed to the detailed comparison of the SED for different objects.

7. SUMMARY AND CONCLUSION

We have explored the IR emission of circumstellar disks in the environment where star formation most typically occurs, i.e., an H II region powered by massive OB stars. This scenario applies in particular to the Orion Nebula, where the interaction of circumstellar disk with the environment has been directly resolved by the *HST*. We have build our model considering the four types of radiation relevant to the dust heating in a H II region, e.g., ionizing (EUV) and nonionizing (FUV) flux from the exciting star (θ^1 Ori C), resonant Lyα radiation and the remaining nebular radiation. We evaluated how these radiation sources affect the IR SED arising from the following:

1. A spherical, homogeneous, optically thin, circumstellar globule, photoevaporated by the UV radiation of the H II region exciting star. The globule has a neutral core of uniform density, and the photoevaporated atmosphere is treated following the Dyson (1968) model. With our assumptions, the most important parameter constraining the IR emission, the radial optical depth to the UV radiation, depends only on the distance from the ionizing star and on the globule size. The thermal emission peaks in the range 10–30 μm, depending mostly on the dust composition.
2. A nonaccreting disk directly exposed to the nebular radiation. The disk is in hydrostatic and radiative equilibrium and is treated following the prescription of CG97. We modify the CG97 scheme to account for the fact that the nebular radiation hits the disk surface with large angles. We follow the propagation of the various radiative fluxes through the disk superheated atmosphere, deriving the vertical temperature profile of the disk atmosphere. The disk faces receive unequal amount of radiation and present different flaring angles. In particular, the flux emitted from the face opposite to the ionizing star provides a model to the IR emission of the dark silhouette disks observed in the Orion Nebula.
3. A combined system composed by the disk and the photoevaporated envelope, i.e., a photoionized proplyd of the type observed in the immediate surroundings of θ^1 Ori C in the Orion Nebula.

Depending on the distance and on the tilt angle of the disk with respect to the ionizing star, the disk flaring may be substantially higher than in the case of isolated disks. The tilt angle with respect to the Earth plays also a major role by hiding the central parts of the disk. The relative intensity of the disk versus envelope emission varies with the tilt angle to the direction of the Earth. The high temperatures reached by the dust either at the disk atmosphere or within the envelope produce a SED peaking at 30–60 μm.

We explore the dependency of the SEDs upon the tilt angle with respect to the Earth, the distance from the ionizing star, the size on the envelope, the inner disk radius, and the temperature of the disk's central star. The resulting SEDs are characterized by a broad peak of emission at 30–60 μm and are in general significantly different from those of isolated disks in low-mass star-forming regions like Taurus-Auriga. Our model indicates that in the presence of an external radiation field, relatively evolved Class 2 objects may

display a SED peaking at mid-IR and far-IR wavelengths. The model explains the strong mid-IR excess we have recently detected on several sources in a 10 μm survey of the Orion Nebula.

The authors whish to thank Bob O'Dell and an anonymous referee for careful reading of the original manuscript and useful comments.

REFERENCES

Bally, J., O'Dell, C. R., & McCaughrean, M. J. 2000, AJ, 119, 2919
Bally, J., Sutherland, R. S., Devine, D., & Johnstone, D. 1998a, AJ, 116, 293
Bally, J., Testi, L., Sargent, A., & Carlstrom, J. 1998b, AJ, 116, 854
Beckwith, S. V. W., & Sargent, A. I. 1996, Nature, 383, 139
Butner, H. M., Natta, A., & Evans, N. J., II, 1994, ApJ, 420, 326
Chiang, E. I., & Goldreich, P. 1997, ApJ, 490, 368
Choi, P., & Herbst, W. 1996, AJ, 111, 283
Dyson, J. E. 1968, Ap&SS, 1, 388
Edwards, S., et al. 1993, AJ, 106, 372
Hartmann, K. 1998, Accretion Processes in Astrophysics (Cambridge: Cambridge Univ. Press), 157
Hayward, T. L., Hock, J. R., & Miles, J. W. 1994, ApJ, 433, 157
Hayward, T. L., & McCaughrean, M. J. 1997, AJ, 113, 346
Henney, W. J., Raga, A. C., Lizano, S., & Curiel, S. 1996, ApJ, 465, 216
Hillenbrand, L. 1997, AJ, 113, 1733
Hummer, D. G., & Kunasz, P. B. 1980, ApJ, 236, 609
Jäeger, C., Mutschke, H., Begemann, B., Dorschner, J., & Henning, Th. 1994, A&A, 292, 641
Johnstone, D., Hollenbach, D., & Bally, J. 1998, ApJ, 499, 758
Kenyon, S. J., & Hartmann, L. 1987, ApJ, 322, 393
Marcy, G. W., Cochran, W. D., & Mayor, M. 2000, in Protostars and Planets IV, ed. V. Manning, A. P. Boss, & S. R. Russell (Tucson: Univ. Arizona Press), 1285
McCaughrean, M. J., & Gezari, D. Y. 1991, in ASP Conf. Ser. 14, Astrophysics with Infrared Arrays, ed. R. Elston (San Francisco: ASP), 301
McCaughrean, M. J., Stapelfeldt, K. R., & Close, L. M. 2000, in Protostars and Planets IV, ed. V. Manning, A. P. Boss, & S. R. Russell (Tucson: Univ. Arizona Press), 485
McCaughrean, M. J., & Stauffer, J. R. 1994, AJ, 108, 1382
McCaughrean, M. J., et al. 1998, ApJ, 492, L157
Natta, A. 1993, ApJ, 412, 76
Natta, A., & Panagia, N. 1976, A&A, 50, 191
O'Dell, C. R. 2001a, ARA&A, 39, 99
———. 2001b, PASP, 113, 209
O'Dell, C. R., & Yusef-Zadeh, F. 2000, AJ, 120, 382
Osterbrock, D. E. 1989, Astrophysics of Gaseous Nebulae and Active Galactic Nuclei (Mill Valley: University Science Books)
Palla, F., & Stahler S. W. 1999, ApJ, 525, 772
Panagia, N. 1973, AJ, 78, 929
———. 1974, ApJ, 192, 221
———. 1978, in Infrared Astronomy, ed. G. Setti & F. Fazio (Dordrecht: Reidel), 115
Pastor, J., Cantó, J., & Rodriguez, L. F. 1991, A&A, 246, 551
Rebull, L. M. 2001, AJ, 121, 1676
Ruden, S. P., & Pollack, J. B. 1991, ApJ, 375, 740
Shakura, N. I., & Sunyaev, R. A. 1973, A&A, 24, 337
Shu, F., Adams, F. C., & Lizano, S. 1987, ARA&A, 25, 23
Stassun, K. G., Mathieu, R. D., Mazeh, T., & Vrba, F. J. 1999, AJ, 117, 2941
Störzer, H., & Hollenbach, D. 1999, ApJ, 515, 669